# Multiscale Elastic Models of Collagen Bio-structures: From Cross-Linked Molecules to Soft Tissues

**Michele Marino and Giuseppe Vairo**

**Abstract** Mechanics of collagen bio-structures at different scales (nano, micro, and macro) is addressed, aiming to describe multiscale mechanisms affecting the constitutive response of soft collagen-rich tissues. Single-scale elastic models of collagen molecules, fibrils, and crimped fibers are presented and integrated by means of consistent inter-scale relationships and homogenization arguments. In this way, a unique modeling framework based on a structural multiscale approach is obtained, which allows to analyze the macroscale mechanical behavior of soft collagenous tissues. It accounts for the dominant mechanisms at lower scales without introducing phenomenological descriptions. Comparisons between numerical results obtained via present model and the available experimental data in the case of tendons and aortic walls prove present multiscale approach to be effective in capturing the deep link between histology and mechanics, opening to the possibility of developing patient-specific diagnostic and clinical tools.

## 1 Introduction

Soft tissues are throughout the whole human body and they include tendons, ligaments, skin, fibrous tissues, muscles and blood vessels. They link, support, and are part of other bio-structures and organs, playing a key role in the biomechanics

M. Marino (✉) · G. Vairo
Department of Civil Engineering and Computer Science, University of Rome "Tor Vergata", via del Politecnico 1, 00133 Rome, Italy
e-mail: m.marino@ing.uniroma2.it

G. Vairo
e-mail: vairo@ing.uniroma2.it

Stud Mechanobiol Tissue Eng Biomater (2013) 14: 73–102
DOI: 10.1007/8415_2012_154

Published Online: 5 October 2012

of many body systems (e.g., musculo-skeletal, cardiovascular) [1]. Collagen, elastin and ground substance are the main constituents of the extracellular matrix in soft tissues, and their arrangement significantly affect the tissue mechanical response. For instance, stiffness and strength features in soft tissues mainly depend on the arrangement and the amount of collagen, which is organized in agreement with a precise hierarchical multiscale scheme [2]. Since the fundamental mechanical role of collagen, soft tissues are usually referred to as collagenous tissues.

The structured organization of soft tissues, and thereby their mechanical behavior, is highly related to the biochemical processes occurring within them [2]. In fact, altered tissue response in disease (e.g., aneurism, keratoconus, arthofibrosis) arises from pathological tissue remodeling, inducing unphysiological histology and biochemical composition. Typical disorders, such as tissue hyper-extensibility or weakness, can be associated with alterations at different scales [3–7]: in content of tissue constituents, in shape of collagen fibers, in collagen genetic pattern, in density of inter-molecular cross-links. Nevertheless, available non-invasive techniques do not allow to measure directly a number of important histological, mechanical, and biochemical properties of collagenous tissues such as, for instance but not exclusively, collagen content and fiber waviness, collagen cross-linking, elastin amount and stiffness of elastin networks.

In this context, the biomechanical analysis and modeling of collagen-rich tissues can be retained a frontier challenge aiming to understand many physiopathological processes occurring at very different length scales, as well as to identify relationships among alterations and diseases. Accordingly, dominant mechanisms occurring at different scales should be accounted for and consistently coupled in a unique modeling approach. Moreover, in order to enhance model reliability for diagnostic and clinical practice, model parameters should be few and associated with clear physical properties of the tissue, avoiding to introduce phenomenological descriptions. These requirements can be satisfied if the tissue structured hierarchical arrangement is explicitly described, possibly reducing model complexity by means of multiscale homogenization techniques. Such an approach, employed for example in [8], will be referred to as a structural multiscale method, and consists in developing mechanical models at very different length scales, which are coupled each other by means of consistent inter-scale relationships. In some way, the structural multiscale approach exploits the rationale followed by nature in “designing“ tissues and “building” organs.

Structural multiscale models open to the possibility of developing virtual simulation tools, that are patient-specific not only for the geometric description of the tissue domains, but also for the accurate representation of the tissue mechanical properties. As a result, the effects of changes in histological arrangement or biochemical processes on the overall macroscopic functionality of tissues and organs could be predicted. Thereby, really customized pharmacological treatments and therapeutic strategies could be conveniently designed and applied. Finally, parametric biomechanical simulations of tissues and organs based on a multiscale structural framework might be coupled with non-invasive in vivo histological and

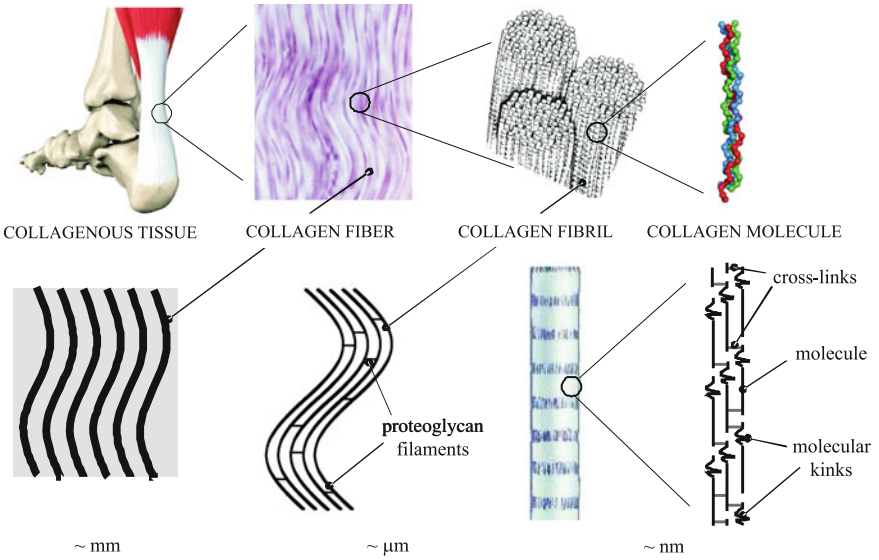


**Fig. 1** Hierarchical arrangement of collagen in a regular soft tissue such as a tendon

functional measures. Accordingly, following an inverse-like scheme, indirect estimates of histo-mechano-chemical features, otherwise unknown, could be furnished aiming to improve diagnostic procedures.

## 2 Biochemical, Histological and Mechanical Properties

Collagen in soft collagenous tissues is arranged according to a precise hierarchical pattern, based on a number of different bio-structures characterized by very different length scales (Fig. 1): from the nanoscale (molecules), to the microscale (fibers), up to the macroscale (tissue). Biomechanics of a single-scale bio-structure and inter-scale coupling effects strictly depend on biochemical, histological and mechanical features at the different scales, and highly affect tissue mechanics at the macroscale.

### *2.1 Collagen Molecules and Fibrils*

The collagen molecule subunit (tropocollagen) can be regarded as a one-dimensional structure about 300 nm long and 1–2 nm in diameter, made up of three polypeptide strands, each one being a left-handed helix. The three helices are twisted together into a triple helix (namely, a "super helix"), representing a cooperative quaternary structure stabilized by covalent cross-links [1].

In collagenous soft tissues, collagen molecules are mainly of type I and they exhibit hydroxyproline-deficient sequences characterized by 60 residues (about 20 nm long), referred to as labile domains and indicated as molecular kinks [2]. Their measure of length $\ell_{kinks}$ is comparable with the value of the persistence length[1] $\ell_p$ for collagen (about 14 nm). This evidence confirms that molecular kinks are activated by thermal fluctuations [2, 9] and can be extended by forces at molecular ends that counteract thermal undulations. In this case entropic mechanisms are activated and a transition regime is experienced, from less ordered molecular states (thermally-activated kinks) to more ordered ones (nearly straight macromolecule). In this regime, usually referred to as entropic elasticity [9], the mechanical response of collagen macromolecules is mainly dominated by the flexural behavior of the polypeptide helices rather than by the extensibility of intra-molecular covalent bonds. Accordingly, neglecting any stretching effect of the intra-molecular bonds and in agreement with the Worm-Like Chain (WLC) model [10, 11], the pair of equilibrated forces $F^s$ to be applied at molecular ends for obtaining the end-to-end molecular length $\ell_m$ results in:

$$F^s(\ell_m) = \rho \left[ \frac{1}{4(1-\ell_m/\ell_c)^2} - \frac{1}{4} + \frac{\ell_m}{\ell_c} \right], \tag{1}$$

where $\ell_c$ is the molecular contour length and $\rho = k_B T/\ell_p$, $T$ being the absolute temperature and $k_B$ the Boltzmann constant. Equation (1) exhibits a pole for $\ell_m = \ell_c$, highlighting that the WLC-model is not able to capture an extension of the end-to-end molecular length over $\ell_c$ involving entropic mechanisms only. Nevertheless, well-established evidences on collagen show a significant level of molecular extensibility beyond $\ell_c$ [12]. Accordingly, when $\ell_m$ approaches $\ell_c$ the applied force contributes to activate the stretch of molecular covalent bonds, inducing the onset of energetic mechanisms [9, 11].

Theoretical models accounting for the extensibility of biopolymer macromolecules over $\ell_c$ have been recently proposed in [13–15], and the transition regime from entropic towards energetic elasticity for collagen has been numerically investigated by using Molecular Dynamical Simulations (MDSs) [9]. MDS-based results proposed in [9] have been successfully recovered by the theoretical approach developed in [15], wherein the transition mechanisms were consistently described by a physically-based lumped-parameter equilibrium formulation, avoiding phenomenological transition parameters as made in [13, 14].

It is worth pointing out that, as experimental [12] and MDS-based [9, 16] results suggest, the mechanical response of collagen molecules due to energetic effects is highly non-linear in the first stage, following a pseudo-exponential law, and then tends asymptotically towards a linearly elastic behavior for $\ell_m \gg \ell_c$. Such an evidence can be justified by observing that the non-linearities are essentially due to

[1] The persistence length is the maximum contour length over which the corresponding molecular segment appears as straight under thermal fluctuations.

the unrolling mechanisms of the triple helical structure, that tends to disappear when $\ell_m \gg \ell_c$. In the literature, both linearly [8, 9] and non-linearly [15] elastic models aiming to describe collagen energetic elasticity can be found.

In biological soft tissues, a single tropocollagen subunit self-assembles in the extracellular matrix with four other collagen molecules, with regularly staggered ends, to form units that in turn assemble themselves into even larger arrays, called fibrils. A collagen fibril, characterized by a diameter between 50 and 500 nm, can be thought as a mesoscale structure between molecule at the nanoscale and fiber at the microscale. Within this organized bio-structure, molecules interact each other by means of both inter-molecular covalent cross-links (each of them connecting two molecules) and weak bonds (including hydrogen bonds and other electromagnetic weak interactions), the former being dominant with reference to the fibril's elastic behavior [17].

Recent experimental evidences [18] revealed a three-dimensional crystallographic patterns of collagen molecules within fibrils. Nevertheless, simple arrangement models were proved to be effective in capturing the mechanical key aspects of fibrils, related to molecules and to their mutual interactions. For instance, according to the Hodge–Petruska scheme [19], fibrils can be successfully modelled as staggered arrays of parallel macromolecules with an axial offset of about 67 nm and an equilibrium center-to-center distance of about 1.5 nm between two transversally adjacent molecules.

## 2.2 Collagen Fibers and Soft Collagenous Tissues

Collagen fibrils are densely packed in bundles called fibers. Adjacent fibrils within fibers are stabilized by lateral fibril-to-fibril proteoglycan filaments [20]. As confirmed by the specialized literature, a controversial matter is if proteoglycans play or not a significant role in loading transfer among adjacent fibrils. If fibers consisted in chains of short fibrils interconnected by proteoglycans, then the among-the-fibrils load-transfer mechanisms would be highly affected by inter-fibrils links [21]. Nevertheless, many recent experimental studies [22, 23] reveal extremely few fibril ends, not confirming the thesis of short fibrils. Moreover, other experimental/numerical results suggest that proteoglycan-based cross-links have a marginal and unlikely mechanical role in the elastic behavior of a collagen fiber [24], although they contribute to fundamental physiological processes. Accordingly, these evidences support the hypothesis that the load-transfer mechanism among fibrils within fibers is nearly proteoglycan-independent.

Soft collagenous tissues are generally fibrous connective tissues which can be either dense or loose, depending on the collagen amount; they consist primarily of elastin, amorphous ground substance, cells and collagen fibers [25]. Collagen fibers can be arranged in agreement with a regular (e.g., tendons) or an irregular (e.g., skin) pattern, and regular tissues (that is, with a regular fiber arrangement) can be conveniently classified in uni- (e.g., tendons and ligaments) or multi- (e.g., arterial

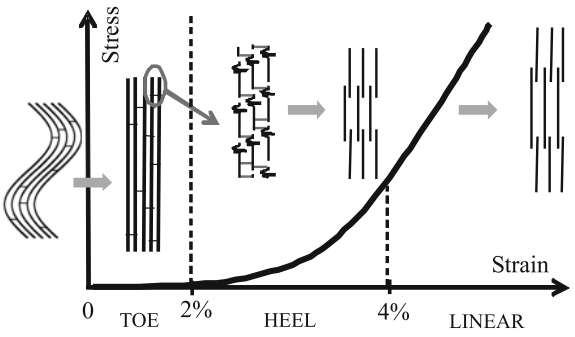


**Fig. 2** Typical stress/strain curve for unidirectional regular soft collagenous tissues such as tendons and ligaments

walls) directional. A multi-directional tissue is intended to be made up of a number of stacked thin layers, each of them with a regular uni-directional fiber arrangement.

As confirmed by well-established studies [2], constitutive response of soft collagenous tissues depends primarily on the mechanical behavior of collagen fibers and molecules. For instance, in the case of a uni-directional tissue subjected to a uni-axial tensile test along the fiber direction, a progressive fiber straightening and the disappearance of nanoscale kinks within molecules are experienced, resulting in an increase of the overall tissue stiffness. Accordingly, the stress/strain curves are typically J-shaped and can be subdivided into three main regions (Fig. 2):

- Toe region: the region of small tissue strains (up to 2 %), related to the removal of the microscopic crimp in collagen fibers.
- Heel region: at strains 2–4 %, characterized by a significant stiffening response due to the entropic straightening of nanoscale molecular kinks [2, 9].
- Linear region: when the tissue is stretched beyond the heel region, most kinks are straightened and no further extension is possible by entropic mechanisms. Therefore, the mechanical response is primarily affected by the stretching of the collagen triple-helices and by molecular rearrangement (collagen sliding) [26].

It should be pointed out that, despite of similar features at the nanoscale, different types of collagenous tissues can be characterized by significantly different mechanical responses, mainly depending on histological composition and organization at lower scales. In the following, two different regular soft collagenous tissues, with different complexity in terms of collagen arrangement, geometry and loading conditions, will be addressed: tendons and the tunica media of the aortic walls.

### 2.2.1 Tendons

Tendons are regular dense connective tissues, transmitting muscular forces and playing a crucial role in the functioning of joints and musculo-skeletal system. The mean axis of collagen fibers in tendons is mainly aligned along the loading

direction, and their geometric features depend on the animal species. For instance, addressing rat tail tendons, collagen fiber crimp period and amplitude are in the order of 200 and 10 μm, respectively [27, 28], and fiber radius varies between 2 and 15 μm [29] (while in humans it can be as high as 300 μm). Finally, collagen volume fraction has been reported to be about 50 % [30], with a little variability depending on tendon location and on physiological conditions.

Due to collagen content and organization, uni-axial tendon stress/strain curves are J-shaped, exhibiting the highly non-linear mechanical response that has been previously described (Fig. 2).

### 2.2.2 Aortic Wall

The aorta is the largest artery in the body, and its structure and mechanical response have a crucial role in the fluid-structure interaction mechanisms relevant to the cardiovascular system. The walls of the aorta are made up of three different tissue layers: a thin inner layer (intima), a thick elastic middle layer (media), and a thin outer layer (adventitia). Among these layers, the media is the most important from the mechanical point of view, as a result of its thickness and stiffness. Histologically, the tunica media is made up of concentric layers consisting in smooth muscle cells embedded in an organized network of loose connective tissue. Many authors (e.g., [31, 32]) describe the media tissue as a thick cylinder comprising different layers, usually denoted as medial lamellar units (MLUs), that have practically the same structural arrangement.

Geometrical features of the aortic media are extremely variable among different living species, depending on the animal size and weight, as well as on the location along the vessel length (e.g., in the thoracic—T—or abdominal—A—zones). Referring to humans, many authors (e.g., [31, 33–35]) indicate that the aortic radius at zero pressure is about 6–9 mm (T) or 5–8 mm (A), that the media thickness-to-radius ratio is about 0.1–0.2, and that the MLU number is about 60 (T) or 30 (A). The three-dimensional histological structure of a single MLU has been recently investigated [36] and described as a thick sub-layer of elastin sided by an interlamellar substance made up of water, elastin, smooth muscle cells and collagen. Collagen results in about 20–30 % of the aortic wall dry-weight [37] and is organized in crimped fibrils with radius varying from 25 to 50 nm [38]. Fibrils are in turn arranged in both thick and thin bundles (namely, fibers). Analysis by means of scanning electron microscopy reveals fiber period in the order of 5 μm and fiber amplitude-to-period ratio about 0.2–0.5 [36]. Fibers are organized in such a way that no complex mesh within each interlamellar layer appears, but they are disposed to realize sub-layers with a uni-directional regular character. In other words, fibers are arranged in circumferential laminae with the fiber axis helically wrapped around the vessel direction, with the wrapping angle (i.e., the angular deflection of the fiber axis with respect to the vessel axis) varying across the MLU thickness, in agreement with a multi-directional tissue structure. Histological evidences [36] confirmed that the wrapping angle exhibits a symmetric uni-modal

distribution with a mean angle of about 90° (i.e., the mean fiber axis direction corresponds to the circumferential's). Regarding such a distribution as a Gaussian one, the full width at half maximum is about 40° and then, in agreement also with sequential confocal microscopic images [36], a variation of the wrapping angle (from the inner towards the outer side of a single lamellar unit) from about 90° up to 70° and from about 90° up to 110° is experienced.

From a mechanical point of view, this complex collagen organization results in a tissue constitutive response highly non-linear, characterized by a progressive stiffening for values of the circumferential strains that increase from the zero-load state. It should be remarked that aortic segments in living bodies are pre-stressed and pre-stretched under zero loads. In fact, when the vessel is excised, the aortic segment shortens, and when a ring cross-section of an artery free of external loads is cut radially, an open sector appears [39–41]. Longitudinal pre-stretch and/or pre-stress generally increases along the length of the aorta, whereas the circumferential one smoothly varies along the longitudinal direction of the vessel.

## 3 Modeling Approaches

At the macroscopic level, several constitutive models for collagen-rich tissues can be found in the specialized literature. Most of them are deduced from phenomenological evidences and generally employ exponential and power-law functions [42, 43], based on parameters having no direct physical or morphological meaning. Other approaches, namely structural approaches, aim to link model parameters with structural properties of the tissue, either by micro–macro homogenization techniques, describing effects related to collagen fibers as linearly elastic [44–46], or by assuming an orthotropic hyper-elastic macroscopic behavior, accounting for the main constituents of the tissue and for some microscale features [47–49]. In this case, non-linearities related to the mechanical response of tissue constituents (mainly geometric non-linearities related to the fiber crimp, and material non-linearities induced by nanoscale mechanisms within and among collagen molecules) are often taken into account by choosing a suitable representation of the fiber strain-energy density (as in a phenomenological approach). Therefore, any direct relationship with the molecular scale is usually neglected and the corresponding models are not able to give predictive indications on nanoscale effects, that probably play the most important role in many diseases (e.g., cross-linking variations are strictly related to aortic rupture and tendon hyper-extensibility [3–7]). Analogously, some microscale features (such as the crimp shape or the thickness of collagen fibers) are not explicitly modeled in many cases, despite of their physiopathological importance (e.g., spontaneously ruptured tendons show reduced thickness and crimp angle [7]).

On the other hand, in a patient-specific framework that aims to give predictive diagnostic indications as well as to describe the tissue response evolution, each model parameter should be directly associated with in vivo measurable features.

This can be obtained by means of a structural multiscale technique, coupling a structural rationale with multiscale homogenization approaches. Accordingly, the equivalent responses of tissue substructures at different scales are analytically derived and consistently integrated, allowing to include at the macroscale the dominant mechanisms occurring at smaller scales [8, 50].

In this context, the authors recently proposed elastic constitutive models for collagen-rich tissues, based on multiscale homogenization techniques that explicitly incorporate nanoscale and microscale mechanisms, as well as their coupling effects [8, 51, 52]. By simulating histological alterations at nano, micro and macro scales, present models have been proved to be able to highlight and to analyze the deep link between histology and mechanical response of both collagenous tissues and body structures [52, 53]. Such an approach allows also to include, through convex analysis arguments and in the same modeling framework, damage evolution at different scales, induced by both mechanical and non-mechanical sources [15].

In the following, a mechanical model of soft collagenous tissues is discussed, addressing the purely elastic response and neglecting any inelastic and damage mechanism. The model generalizes the one proposed and applied in [8, 51], and follows a structural multiscale rationale. The macroscale tissue response is recovered by integrating single-scale models of collagenous bio-structures at very different length scales: molecules (nanoscale), fibrils (mesoscale) and crimped fibers (microscale). Following a structural approach, the ordered histology of both uni-directional and multi-directional tissues is explicitly taken into account.

As a result of a multi-step homogenization procedure, the homogenized tissue at the macroscale is treated as a non-linearly elastic anisotropic continuum, passing from its reference configuration to the actual one via a quasi-static deformation path $\phi$, governed by a time-like variable $\tau$. In turn, bio-structures at lower scales undergo to $\phi$-induced quasi-static transformations. At each scale this process is herein described following an incremental strategy. For the sake of notation, in what follows the symbol $\dot{x}$ denotes the partial derivative of $x$ with respect to $\tau$.

## 4 Nanoscale Mechanics: Molecules

A collagen molecule is modelled as an equivalent zero-dimensional nano-structure, whose reference end-to-end length is $\ell_{m,o}$, and is lower than its contour length $\ell_c$. Let $A_m$ be a measure of the molecular cross-sectional area (assumed to be constant during the overall deformation process), and $\varepsilon_m = \ell_m/\ell_{m,o} - 1$ a measure of the molecular nominal strain, $\ell_m$ being the actual molecular end-to-end length.

Entropic and energetic mechanisms are assumed to act as in series and they contribute to the overall molecular stretch measure $\varepsilon_m$ by $\varepsilon_m^s$ and $\varepsilon_m^h$, respectively, so that by compatibility

$$\varepsilon_m = \varepsilon_m^s + \varepsilon_m^h. \tag{2}$$

Denoting with $r_\ell = \ell_{m,o}/\ell_c$, the molecular tangent modulus $E_m^s$ that describes the entropic mechanisms can be introduced, in agreement with the WLC model [8], as

$$E_m^s(\varepsilon_m^s) = \frac{\rho}{A_m}\left\{\frac{r_\ell}{2[1 - r_\ell(1 + \varepsilon_m^s)]^3} + r_\ell\right\}. \tag{3}$$

Moreover, the molecular tangent modulus $E_m^h$ dealing with energetic mechanisms is represented as [15]:

$$E_m^h(\varepsilon_m^h) = \frac{\hat{E} r_\ell}{1 + e^{-\eta(r_\ell \varepsilon_m^h - \varepsilon_o^h)}} + \hat{E}_o r_\ell, \tag{4}$$

where $\hat{E}$, $\hat{E}_o$, $\eta$ and $\varepsilon_o^h$ are model parameters.

Expression (4) is able to grasp the experimental evidence that the molecular mechanical response is characterized in the first stage by a pseudo-exponential law, and then asymptotically tends to a linearly elastic behavior for high values of $\ell_m/\ell_c$. The introduced parameters have a clear physical meaning and, thereby, their values can be set by numerical atomistic computations or, when available, by experiments: $\hat{E}$ and $\hat{E}_o$ govern the asymptotic behavior of $E_m^h(\varepsilon_m^h)$ for $\varepsilon_m^h \to \pm\infty$, $\eta$ describes the slope of the function $E_m^h(\varepsilon_m^h)$ for $\varepsilon_m^h = \varepsilon_o^h$, and $\varepsilon_o^h$ is the molecular strain contribution within the energetic regime at which $E_m^h$ practically attains its mean value.

Therefore, the molecular tangent modulus accounting for the series elasticity induced by entropic and energetic mechanisms results in:

$$E_m(\varepsilon_m) = \frac{E_m^s(\varepsilon_m^s) E_m^h(\varepsilon_m^h)}{E_m^s(\varepsilon_m^s) + E_m^h(\varepsilon_m^h)}, \tag{5}$$

and the strain contributions due to entropic and energetic effects, that is the functions $\varepsilon_m^s = \varepsilon_m^s(\varepsilon_m)$ and $\varepsilon_m^h = \varepsilon_m^h(\varepsilon_m)$, are obtained by solving the following differential problem:

$$\dot{\varepsilon}_m^s = \frac{E_m(\varepsilon_m)\dot{\varepsilon}_m}{E_m^s(\varepsilon_m^s)}, \qquad \dot{\varepsilon}_m^h = \frac{E_m(\varepsilon_m)\dot{\varepsilon}_m}{E_m^h(\varepsilon_m^h)}. \tag{6}$$

Accordingly, the description of the entropic/energetic transition directly derives from the mutual competition of the stiffnesses associated to $E_m^s$ and $E_m^h$: when $E_m^s \ll E_m^h$ molecular mechanics is mainly governed by the entropic mechanisms ($E_m \approx E_m^s$), when $E_m^s \gg E_m^h$ by the energetic ones ($E_m \approx E_m^h$), whereas when $E_m^s \approx E_m^h$ both mechanisms significantly contribute. As the analysis of Eqs. (6) reveals, present model of the entropic/energetic transition is based on equilibrium and compatibility conditions, despite of the phenomenological approaches introduced in [13, 14].

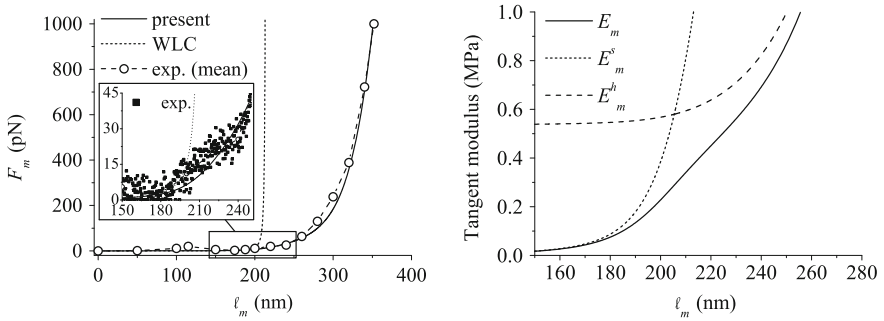


**Fig. 3** *Left*: comparison among $F_m$-$\ell_m$ curves obtained for a collagen molecule by experimental tests [54], classical WLC, and present model. *Right*: molecular ($E_m$), entropic ($E^s_m$), and energetic ($E^h_m$) tangent moduli vs. $\ell_m$ for a collagen molecule. Parameters: $T = 310.15$ K, $\ell_p = 14.5$ nm, $\ell_c = 215$ nm, $\ell_{m,o} = 1$ nm, $\hat{E}_o = 0.1$ GPa, $\hat{E} = 10$ GPa, $\eta = 10$, $\varepsilon^h_o = 0.65$

For the uni-axial traction problem of a collagen molecule, the force pair $F_m$ applied at the molecular ends can be computed in terms of the actual molecular length $\ell_m$ as $F_m = A_m \sigma_m$, where the molecular stress measure results from:

$$\sigma_m(\varepsilon_m) = \int_0^{\varepsilon_m} E_m(\xi) d\xi, \tag{7}$$

$E_m$ being expressed by Eq. (5).

In Fig. 3, the $F_m$-$\ell_m$ curve obtained by means of the present approach is compared with the experimental data proposed in [54] and with results computed by the classical WLC model, that is by employing Eq. (1). As reported by many authors [9, 54], the WLC model fits well the molecular response experienced in a low-force regime, but predicts an unrealistic molecular inextensibility at high forces. On the contrary, the proposed approach exhibits an excellent agreement in the overall force range herein addressed, accounting for the molecular compliance during the entropic/energetic transition. In Fig. 3b the molecular tangent modulus is plotted versus the molecular extension, highlighting that $E_m \approx E^s_m$ within the entropic regime, and $E_m \approx E^h_m$ in the energetic one.

Another verification of consistency and soundness of the proposed model for the entropic/energetic transition follows from Fig. 4a: it shows the computed strain rates $\dot{\varepsilon}^s_m$ and $\dot{\varepsilon}^h_m$ (normalized with respect to $\dot{\varepsilon}_m$) plotted versus the molecular length $\ell_m$. Reference is made to the numerical analyses proposed in [9], wherein for a collagen molecule with $\ell_c = 301.7$ nm, MDS-based results predict that the entropic regime dominates for $\ell_m < 280$ nm and the energetic one for $\ell_m > 317$ nm. This evidence is fully recovered by present results obtained by solving Eqs. (6): $\dot{\varepsilon}^h_m \to 0$ for $\ell_m < 280$ nm and $\dot{\varepsilon}^h_m / \dot{\varepsilon}_m \to 1$ for $\ell_m > 317$ nm. It is worth pointing out that present equilibrium and compatibility conditions ensure that the pole at $\varepsilon^s_m = 1/r_\ell - 1$ for the function $E^s_m(\varepsilon^s_m)$ is never reached ($\dot{\varepsilon}^s_m \to 0$ for $\ell_m > 317$ nm).

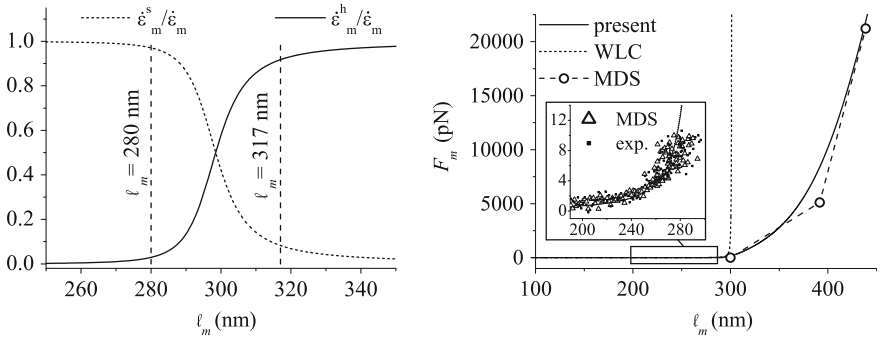


**Fig. 4** *Left*: strain rates associated with entropic ($\dot{\varepsilon}^s_m$) and energetic ($\dot{\varepsilon}^h_m$) mechanisms (normalized with respect to $\dot{\varepsilon}_m$) computed by the present approach. *Right*: collagen $F_m$-$\ell_m$ curves obtained by experimental tests [12], MDS [9], classical WLC, and present model. Parameters: $T = 310.15$ K, $\ell_p = 16$ nm, $\ell_c = 301.7$ nm, $\ell_{m,o} = 1$ nm, $\hat{E}_o = 5$ GPa, $\hat{E} = 100$ GPa, $\eta = 10$, $\varepsilon^h_o = 0.35$

Moreover, in Fig. 4b, the $F_m$-$\ell_m$ curve obtained in this case is successfully compared with the experimental data proposed in [12] (available only for low molecular forces), as well as with the numerical results in [9].

## 5 Mesoscale Mechanics: Fibrils

Collagen fibrils are modelled as long right cylinders. Let **f** be the fibril axis direction, and $A_f$ a measure of the fibril cross-sectional area. From a computational point of view, fibrils are thought as a collection of $N_m$ identical one-dimensional molecules, with axis aligned along **f** and mutually interacting through $N_{cl}$ identical cross-links, which connect pairs of adjacent molecules (see Fig. 5). Molecules in reference configuration are assumed to be long $\ell_{m,o} = \ell_c - \ell_{kinks}$, $\ell_{kinks}$ being the length measure of molecular kinks.

Let $n_s$ be the average number of molecules along the fibril length and $\ell_{f,o}$ the reference fibril length. Disregarding axial offset among molecules, the following relationship holds: $\ell_{f,o} \approx n_s \ell_{m,o}$. Moreover, let $\lambda$ be an average measure of cross-link occurrence for each molecule, such that $N_{cl} = \lambda N_m$. In the case of a homogeneous traction and defining $\delta$ as the sway of a cross-link along the fibril length, it is consistent to assume that both molecular strain $\varepsilon_m$ and cross-link stretch $\delta$ are space-independent quantities within the fibril domain.

Furthermore, denoting with $\Delta\ell_f$ the fibril length variation and with $\varepsilon_f$ the fibril nominal strain, the following kinematic assumption is enforced:

$$\Delta\ell_f = n_s(\ell_{m,o}\varepsilon_m + \delta) \rightarrow \varepsilon_f = \frac{\Delta\ell_f}{\ell_{f,o}} = \left(\varepsilon_m + \frac{\delta}{\ell_{m,o}}\right), \tag{8}$$

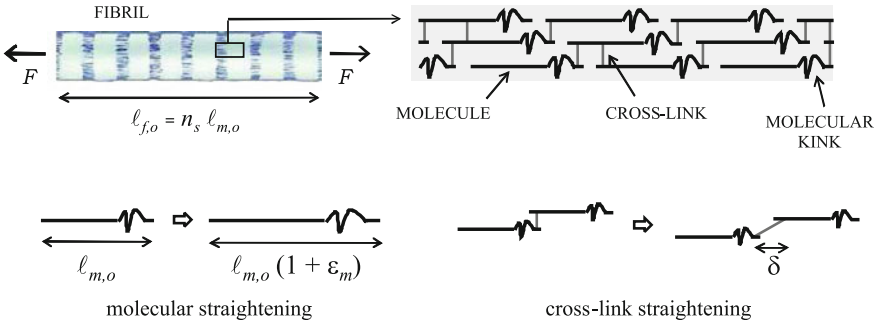


**Fig. 5** Fibril model. Notation

that accounts for series mechanisms occurring between molecular and cross-link stretching, and that is consistent with experimental evidences [26]. It is worth pointing out that parameter $\lambda$ does not intervene in the compatibility equation (8) because covalent cross-links occurring upon a given molecule are assumed to act in parallel.

Assuming a linearly elastic behavior with sway stiffness $k_{cl}$ for each cross-link, a measure of the nominal fibril stress along **f** is

$$\sigma_f = \mu\sigma_m = \lambda k_{cl}\delta/A_f, \tag{9}$$

with $\sigma_m$ expressed by Eq. (7) and where $\mu$ is the average measure of the ratio between solid (occupied by molecules) and total cross-section. Accordingly, by combining Eqs. (8) and (9), the fibril tangent elastic modulus along **f** results in:

$$E_f(\varepsilon_f) = \mu\left[\frac{1}{E_m(\varepsilon_m)} + \frac{A_m}{\lambda k_{cl}\ell_{m,o}}\right]^{-1}, \tag{10}$$

where the contribution to the molecular elongation due to the fibril strain, that is the function $\varepsilon_m = \varepsilon_m(\varepsilon_f)$, is obtained by solving the following inter-scale equilibrium differential problem:

$$\dot{\varepsilon}_m = \frac{E_f(\varepsilon_f)}{\mu E_m(\varepsilon_m)}\dot{\varepsilon}_f. \tag{11}$$

In the following, since fibrils within tissues are made up of densely packed molecules and in agreement with evidences proposed by [55], the model parameter $\mu$ is set equal to one.

In Fig. 6, numerical results obtained considering a uni-axial traction of a collagen fibril are shown, highlighting the capability of the proposed approach to predict the evolution of both molecular and fibril tangent moduli versus $\varepsilon_f$. In agreement with recent theoretical evidences at the atomistic scale [2, 56], lower values of the fibril stiffness with respect to the molecular ones are successfully reproduced, as induced by the stretching of inter-molecular cross-links. Moreover,

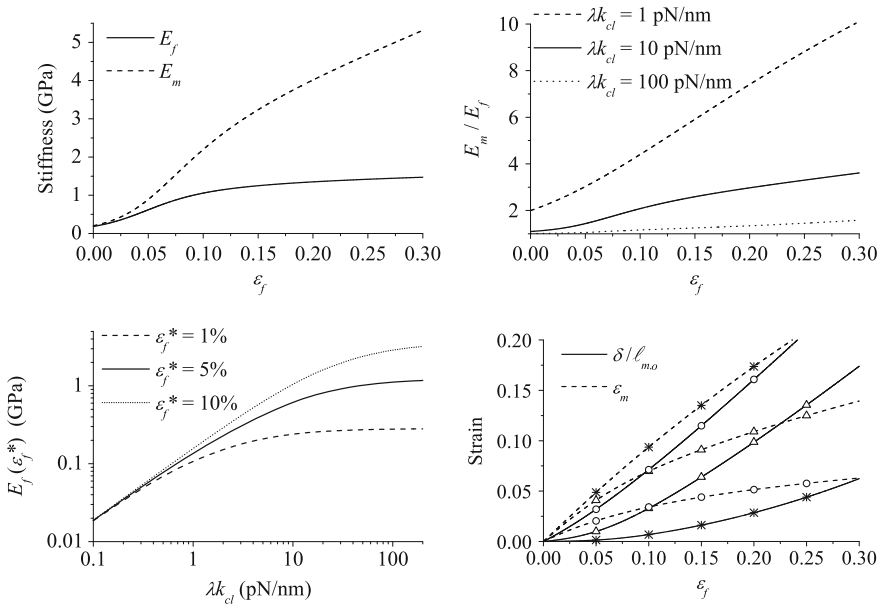


**Fig. 6** *Top left*: fibril ($E_f$) and molecular ($E_m$) tangent moduli vs. fibril nominal strain $\varepsilon_f$ (computed for $\lambda k_{cl} = 10$ pN/nm). *Top right*: ratio between molecular and fibril moduli $E_m/E_f$ vs. fibril nominal strain $\varepsilon_f$ for different values of $\lambda k_{cl}$. *Bottom left*: fibril tangent modulus $E_f$ (in $\log_{10}$ scale) vs. $\lambda k_{cl}$ (in $\log_{10}$ scale) for different values of fibril nominal strain $\varepsilon_f^*$. *Bottom right*: molecular nominal strain $\varepsilon_m$ and cross-link normalized extension $\delta/\ell_{m,o}$ vs. fibril strain $\varepsilon_f$ for different values of $\lambda k_{cl}$: (○) $\lambda k_{cl} = 1$ pN/nm; (△) $\lambda k_{cl} = 10$ pN/nm; (∗) $\lambda k_{cl} = 100$ pN/nm. Constant parameters: $\ell_p = 14.5$ nm, $\ell_c = 287$ nm, $\ell_{kinks} = 22$ nm, $\hat{E}_o = 1$ GPa, $\hat{E} = 100$ GPa, $\eta = 10$, $\varepsilon_o^h = 0.35$, $A_m = 1.41$ nm$^2$, $T = 310.15$ K, $\mu = 1$

a quantitative estimate of the fibril stiffness variation due to changes in cross-link mechanics is provided, showing that fibril stiffness significantly varies both in terms of absolute values and with respect to the molecule's. An increase in cross-link occurrence produces an increase in fibril modulus up to a saturation level that corresponds to the molecular stiffness. Furthermore, numerical results clearly show the non-linear dependence of molecular and cross-link strain measures on both fibril strain and occurrence/stiffness of cross-links.

These results at the mesoscale recover and justify also other significant evidences. Since identical collagen molecules likely exhibit identical nano-mechanical responses, the wide range of values for fibril/fiber modulus, generally reported in the specialized literature as a result of microscale experimental investigations (0.2–12 GPa [2]), can be justified via the proposed results as a consequence of different occurrence and mechanical response of cross-links. Moreover, since after the removal of fibril (fiber) geometrical crimp the mechanical response of the fibrils' material (corresponding to cross-linked collagen molecules) can be considered as representative of the elastic behavior of

the overall tissue [2, 8], present results recover the tissue stiffening experienced at the macroscale, confirming as this occurrence can be associated with the formation of mature cross-links [57, 58].

## 6 Microscale Mechanics: Fibers

A collagen fiber is modeled as a homogeneous beam with a circular cross-section of radius $r_F$ and with a periodic planar centerline in both reference and actual configurations (Fig. 7). Let the along-the-chord nominal strain measure be defined as $\varepsilon_F = L/L_o - 1$, $L$ (respectively $L_o$) being the actual (reference) fiber period. Moreover, let the Cartesian frame $(\mathbf{t}, \mathbf{n})$ be introduced, with the unit vector $\mathbf{t}$ aligned with the actual fiber chord direction, and let $x$ be the coordinate along $\mathbf{t}$. Accordingly, the centerline position vector results in $\mathbf{r}(x, \varepsilon_F) = f(x, \varepsilon_F)\,\mathbf{n} + x\,\mathbf{t}$, where $f(x, \varepsilon_F)$ denotes the centerline curve, whose slope with respect to $\mathbf{t}$ is defined by the angle $\alpha(x, \varepsilon_F)$.

Following a constrained Hu-Washizu variational approach, and disregarding any shear and Poisson-related effect, the tangent equivalent along-the-chord fiber modulus $E_{eq}$ results in [59]:

$$E_{eq}(\varepsilon_F) = E_c I_F \langle \cos\alpha \rangle \left[ I_F \langle \cos^2\alpha \rangle + A_F \langle f^2 \rangle \right]^{-1}, \tag{12}$$

where $E_c$ is the tangent elastic modulus of the fiber material along the direction perpendicular to the fiber cross-section, $A_F = \pi r_F^2, I_F = \pi r_F^4/4$, and symbol $\langle \cdot \rangle$ denotes the curvilinear average operator defined along the curvilinear coordinate $s$ following the fiber centerline, that is

$$\langle \cdot \rangle = \frac{1}{\mathcal{L}(\varepsilon_F)} \int_0^{\mathcal{L}(\varepsilon_F)} \cdot \, ds, \tag{13}$$

$\mathcal{L}(\varepsilon_F)$ being the length over a period of the actual fiber centerline. By assuming the fiber material behavior to be governed by the fibril non-linear constitutive response, that is enforcing the constitutive inter-scale condition $E_c = E_f(\varepsilon_f)$, nano- and mesoscale mechanical effects are straightforwardly included in the mechanical description of a collagen fiber. Nominal strain $\varepsilon_f$ associated with $\varepsilon_F$, that is the function $\varepsilon_f = \varepsilon_f(\varepsilon_F)$, is computed from the following inter-scale compatibility relationship:

$$\varepsilon_f = \mathcal{L}(\varepsilon_F)/\mathcal{L}(0) - 1, \tag{14}$$

with

$$\mathcal{L}(\varepsilon_F) = \int_0^L \frac{d\zeta}{\cos\alpha}. \tag{15}$$

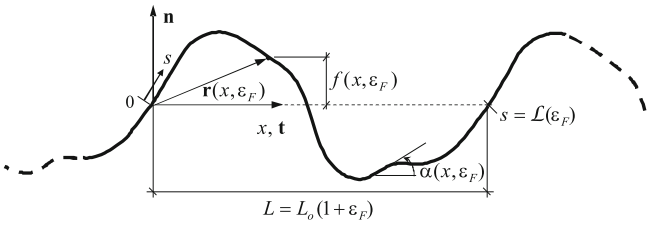


**Fig. 7** Planar fiber model. Notation

The actual shape $f(x,\varepsilon_F)=\mathbf{r}(x,\varepsilon_F)\cdot\mathbf{n}$ at the along-the-chord strain level $\varepsilon_F$ is determined by solving the following differential problem, resulting by applying the Principle of Virtual Works [59]:

$$\dot{\mathbf{r}}(x,\varepsilon_F)=\frac{E_{eq}(\varepsilon_F)}{E_f(\varepsilon_f)}[a_1(x,\varepsilon_F)\,\mathbf{n}+a_2(x,\varepsilon_F)\mathbf{t}]\dot{\varepsilon}_F, \tag{16}$$

with

$$\begin{aligned} a_1(x,\varepsilon_F)=&-x\bar{a}(\varepsilon_F)+\int_0^x\left[\sin\alpha-\frac{A_F}{I_F}\frac{\zeta f}{\cos\alpha}\right]d\zeta\\ &-x\frac{A_F}{I_F}\int_x^L\frac{f}{\cos\alpha}\,d\zeta, \end{aligned} \tag{17}$$

$$\begin{aligned} a_2(x,\varepsilon_F)=&f(x,\varepsilon_F)\bar{a}(\varepsilon_F)+\int_0^x\left[\cos\alpha+\frac{A_F}{I_F}\frac{f^2}{\cos\alpha}\right]d\zeta\\ &+f(x,\varepsilon_F)\frac{A_F}{I_F}\int_x^L\frac{f}{\cos\alpha}\,d\zeta, \end{aligned} \tag{18}$$

$$\bar{a}(\varepsilon_F)=\frac{1}{2\langle\cos\alpha\rangle}\left[\langle\sin 2\alpha\rangle-2\frac{A_F}{I_F}\langle\zeta f\rangle\right]. \tag{19}$$

In order to show effectiveness and soundness of the proposed microscale description, numerical results obtained for an isolated collagen crimped fiber are discussed, addressing the fiber along-the-chord response. The reference centerline curve $f(x,0)$ is defined as the sum of two sinusoidal waves depending on the parameters $\omega\in\mathbb{N}$ ($\omega\geq 0$) and $\chi\in\mathbb{R}$:

$$f(x,0)=H_o\sin(2\pi x/L_o)+\chi H_o\sin(2\omega\pi x/L_o) \tag{20}$$

and, as a notation rule, $H_{max,o}=\max\{f(x,0)\}$. Moreover, nanoscale parameters defining the fiber's material behavior are assumed to be equal to $\ell_p=14.5$ nm, $\ell_c=287$ nm, $\hat{E}_o=1$ GPa, $\hat{E}=100$ GPa, $\eta=10$, $\varepsilon_o^h=0.35$, $\ell_{kinks}=22$ nm, $A_m=1.41$ nm$^2$, $T=310.15$ K, $\mu=1$ and $\lambda k_{cl}=10$ pN/nm.

By integrating Eq. (16), reference and actual (at $\varepsilon_F=0.1$) shapes of curvilinear fibers with different centerline curves are shown in Fig. 8. The typical stiffening

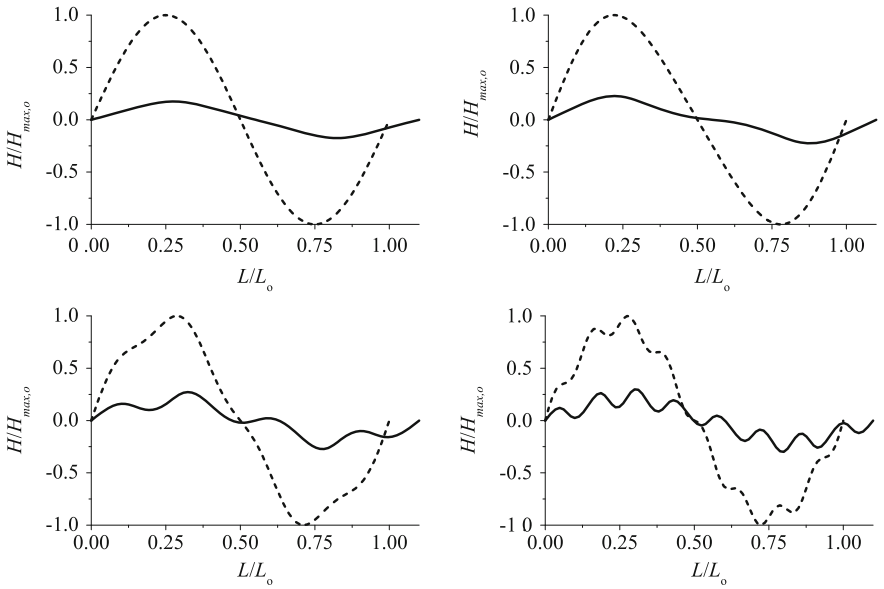


**Fig. 8** Actual fiber configuration at $\varepsilon_F = 0.1$ (*continuous lines*) for different reference centerline shapes (*dotted lines*) corresponding to $\omega = 0$ (*top left*), $\omega = 2$ (*top right*), $\omega = 4$ (*bottom left*), and $\omega = 8$ (*bottom right*). Parameters: $H_o/L_o = 0.1$, $r_F/L_o = 0.025$, $L_o = 100\,\mu\text{m}$, $\chi = 0.1$

response related to the decrease of the fiber crimp is highlighted in Fig. 9, wherein the centerline shape is proved to affect the fiber mechanical response mostly for high values of the aspect ratio $H_o/L_o$, resulting in a significant dependence on the parameters $\chi$ and $\omega$.

The fiber behavior is highly non-linear because of both material (at nanoscale and mesoscale) and geometric effects. Nevertheless, if the equivalent modulus $E_{eq}$ is normalized with respect to the fibril's one $E_f$, the effects related only to geometric non-linearities can be highlighted. Accordingly, Fig. 10 shows the influence of the shape parameters ($H_o/L_o$, $\omega$, and $r_F/L_o$) on the fiber mechanical response related to geometric non-linearities, in terms of the tangent modulus in the reference configuration (i.e., at $\varepsilon_F = 0$) as well as in terms of modulus variation versus the fiber strain level $\varepsilon_F$.

## 7 Macroscale Mechanics

Previous microscale approach is employed to describe the mechanical behavior of collagenous fibers within regular soft tissues. Fibers are assumed to be embedded into a linearly elastic isotropic matrix, whose Young modulus and Poisson ratio are $E_M$ and $\nu_M$, respectively. Neglecting any fiber–matrix interaction effect, crimped fibers are reduced to equivalent reinforcing straight fibers, exhibiting an elastic

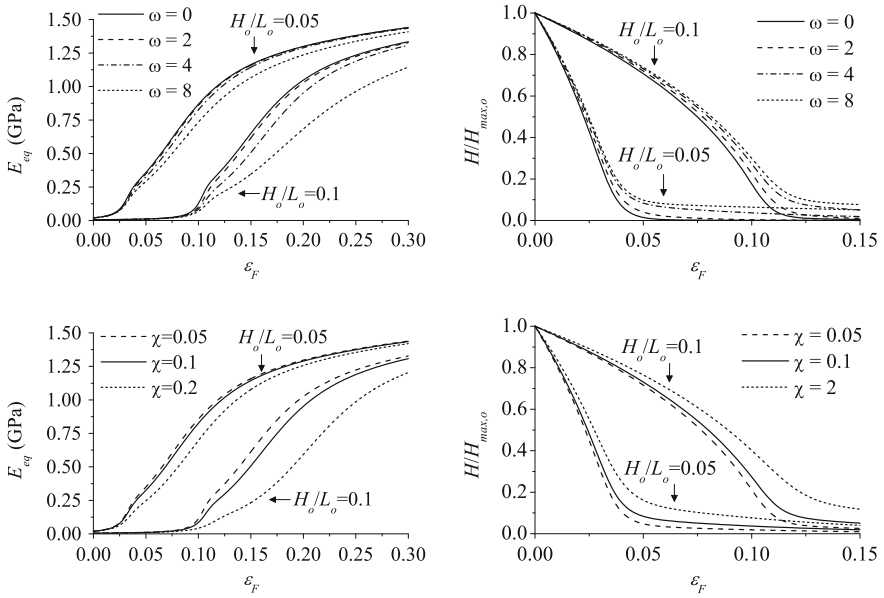


**Fig. 9** Along-the-chord modulus $E_{eq}$ (*left*) and dimensionless amplitude variation $H(\varepsilon_F)/H_{max,o}$ (*right*) vs. the fiber along-the-chord nominal strain $\varepsilon_F$ for different reference centerline curves. Parameters: $r_F/L_o = 0.025$, $L_o = 100\,\mu\text{m}$, $\chi = 0.1$, $\omega = 4$

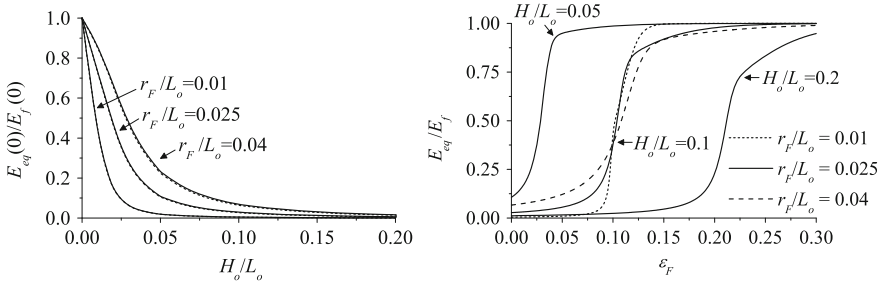


**Fig. 10** Influence of the aspect ratios $H_o/L_o$ and $r_F/L_o$ on the fiber mechanical response. *Left*: Along-the-chord modulus $E_{eq}$ at $\varepsilon_F = 0$, normalized with respect to the initial fibril modulus $E_f(0)$ for different reference centerline geometries ($\omega = 0$: *continuous line*; $\omega = 8$: *dotted line*). *Right*: Along-the-chord modulus $E_{eq}$ normalized with respect to the fibril modulus $E_f(\varepsilon_f)$ vs. the nominal fiber strain $\varepsilon_F$ for $\omega = 4$. Parameters: $L_o = 100\,\mu\text{m}$, $\chi = 0.1$

transversally isotropic behavior with the symmetry axis coincident to the fiber-chord direction **t**. Due to the small values of the fiber flexural stiffness and of $E_M$ [9], the Poisson ratio ($\nu_F$), the tangent tensile ($E_F$) and the shear ($G_F$) elastic moduli of an equivalent fiber within the tissue are represented by:

$$E_{F,L}(\varepsilon_F) = E_{eq}(\varepsilon_F), \qquad E_{F,T} = E_M, \tag{21}$$

$$\nu_{F,LT} = \nu_{F,TT} = \nu_M, \qquad G_{F,LT} = E_M/[2(1+\nu_M)], \tag{22}$$

with $E_{eq}(\varepsilon_F)$ as in Eq. (12) and where the subscript $L$ refers to the direction identified by **t**, whereas $T$ to any direction orthogonal to **t**.

Once crimped collagenous fibers are reduced to equivalent straight fibers, through the previous homogenization step and accounting for geometrical and material non-linearities, standard arguments for fiber-reinforced composite materials can be employed in order to describe the macromechanics of soft collagenous tissues.

## 7.1 Uni-directional Tissues: Tendons and Ligaments

A further homogenization step at the macroscale is carried out by employing the mixture rule [60]. Accordingly, a uni-directional collagenous tissue is reduced to a homogeneous medium with a transversally isotropic behavior, the isotropy plane being orthogonal to **t**. Therefore, tangent equivalent elastic constants of the tissue at the along-the-chord fiber strain level $\varepsilon_F$ result in:

$$E_L(\varepsilon_F) = V_f E_{F,L}(\varepsilon_F) + (1-V_f)E_M, \qquad E_T = \frac{E_{F,T}E_M}{E_{F,T}(1-V_f)+E_M V_f}, \tag{23}$$

$$G_{LT} = \left(\frac{V_f}{G_{F,LT}} + \frac{1-V_f}{G_M}\right)^{-1}, \qquad G_{TT} = \left(\frac{V_f}{G_{F,TT}} + \frac{1-V_f}{G_M}\right)^{-1}, \tag{24}$$

$$\nu_{LT} = V_f \nu_{F,LT} + (1-V_f)\nu_M, \qquad \nu_{TT} = \frac{E_T}{2G_{TT}} - 1, \tag{25}$$

where $V_f$ is the fiber volume fraction. Referring to the standard Voigt notation, the tangent stiffness matrix $\tilde{\mathbb{C}}$ in the material coordinate system (**t**,**n**,**k**), with $\mathbf{k} = \mathbf{t} \times \mathbf{n}$, is:

$$\tilde{\mathbb{C}}(\varepsilon_F) = \begin{bmatrix} \mathbb{L}(\varepsilon_F) & 0 \\ 0 & \mathbb{M} \end{bmatrix}, \tag{26}$$

where

$$\mathbb{L}(\varepsilon_F) = \frac{1}{D}\begin{bmatrix} E_L(1-\nu_{TT}^2) & E_T\nu_{LT}(1+\nu_{TT}) & E_T\nu_{LT}(1+\nu_{TT}) \\ E_T\nu_{LT}(1+\nu_{TT}) & E_T(1-\kappa\nu_{LT}^2) & E_T(\nu_{TT}+\kappa\nu_{LT}^2) \\ E_T\nu_{LT}(1+\nu_{TT}) & E_T(\nu_{TT}+\kappa\nu_{LT}^2) & E_T(1-\kappa\nu_{LT}^2) \end{bmatrix}, \tag{27}$$

$$\mathbb{M} = \mathrm{diag}(G_{TT},\ G_{LT},\ G_{LT}), \qquad D(\varepsilon_F) = 1 - \nu_{TT}^2 - 2(1+\nu_{TT})\kappa\nu_{LT}^2, \tag{28}$$

with $E_L = E_L(\varepsilon_F)$ and $\kappa = \kappa(\varepsilon_F) = E_T/E_L(\varepsilon_F)$.

Accordingly, at the macroscale and in a global coordinate system, the tangent homogenized constitutive law for the tissue results in:

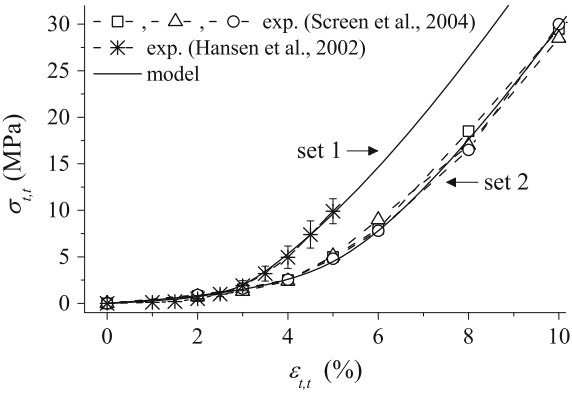


**Fig. 11** Mechanics of uni-directional tissues: experimental along-**t** constitutive response of rat tail tendons [27, 61] compared with the numerical results obtained via present model by using two consistent sets of micro/macro model parameters (Table 1). $\sigma_{t,t}$ and $\varepsilon_{t,t}$ denote direct stress and strain components, respectively, along the fiber-chord direction **t**. The shape of the collagen fiber centerline in the reference configuration is defined as in Eq. (20) with $\chi = 0$. Values of nanoscale model parameters are set equal to: $\ell_p = 14.5$ nm, $\ell_c = 287$ nm, $\hat{E}_o = 1$ GPa, $\hat{E} = 80$ GPa, $\eta = 22.5$, $\varepsilon_o^h = 0.1$, $\ell_{kinks} = 14$ nm, $A_m = 1.41$ nm$^2$, $T = 310.15$ K, $\mu = 1$, $\lambda k_{cl} = 10$ pN/nm

**Table 1** Values of micro- and macroscale parameters for tendons employed in numerical applications with relevant references

| | $H_o/L_o$ | $r_F/L_o$ | $L_o$ (μm) | $V_f$ | $E_M$ (MPa) | $\nu_M$ |
|---|---|---|---|---|---|---|
| Set 1 | 0.05 | 0.02 | 200 | 50 % | 1 | 0.49 |
| Set 2 | 0.0635 | 0.0325 | | | | |
| Ref. | [28] | [29] | [27, 28] | [30] | [62] | [62] |

$$\dot{\boldsymbol{\sigma}}_t = \mathbb{C}(\varepsilon_F)\dot{\boldsymbol{\varepsilon}}_t = \hat{\mathbb{T}}_\sigma(\mathbf{t})\tilde{\mathbb{C}}(\varepsilon_F)[\hat{\mathbb{T}}_\varepsilon(\mathbf{t})]^{-1}\dot{\boldsymbol{\varepsilon}}_t, \tag{29}$$

where $\hat{\mathbb{T}}_\sigma(\mathbf{t})$ and $\hat{\mathbb{T}}_\varepsilon(\mathbf{t})$ are the stress and strain transformation matrix from the local to the global coordinate system, and $\dot{\boldsymbol{\varepsilon}}_t$, $\dot{\boldsymbol{\sigma}}_t$ are the increments of macro strain and stress vectors (in Voigt notation) for the equivalent homogeneous tissue, respectively.

In order to validate the present approach, uni-axial traction along the fiber-chord direction of tendinous tissues is addressed, comparing available experimental data for rat tail tendons with numerical results obtained via the proposed model. Figure 11 shows the excellent agreement between experimental results measured from two different tendinous specimens [27, 61] and the model's outcomes. These are obtained by using an incremental approach and considering two different sets of parameters (Table 1). The major issue is that, setting the same values for nanoscale parameters (since the collagen-related nanoscale features are similar among different healthy tissues), different tissue mechanical responses are clearly reproduced by considering differences in microscale fiber geometry.

## 7.2 Multi-directional Tissues: The Aortic Media Case

The proposed approach can be also employed to describe multi-layered tissues, comprising layers each having a uni-directional collagen fiber arrangement. This is the case of the arterial tunica media. In the following, reference will be made to the aorta.

Following experimental evidences [31, 32, 36] and well-established modeling approaches [47], aortic media is modelled as a multi-layered thick-walled cylinder (with internal radius $r_i$ and thickness $h_a$) made up of $N$ identical layers (media lamellar units MLUs, see Fig. 12). Such a multi-layered cylinder is assumed to have a length much greater than $r_i$, and to be loaded by a uniform internal pressure distribution $p$, undergoing prevailing membranal response with negligible flexural effects. Let the cylindrical coordinate system $(z, \varphi, \rho)$ be introduced, where $\rho$ is the radial coordinate, and $\varphi$ and $z$ the angular and axial coordinates, respectively.

Each MLU comprises an elastin rich elastic lamina (EL) $h_e$ thick and an interlamellar substance (IL) with thickness $h_{\mathrm{IL}}$.

The EL sub-layer is modelled as a two-phase substance comprising void (or very soft constituents with negligible stiffness) with volume fraction $V_o$, and elastin. The latter is assumed with a linearly elastic isotropic behavior and characterized by the Young's modulus $E_e$ and the Poisson's ratio $v_e$. Accordingly, EL can be reduced by the mixture rule to a homogeneous layer with equivalent isotropic elastic constants equal to $(1 - V_o)E_e$ and $(1 - V_o)v_e$.

The interlamellar substance, in turn, can be regarded as a multi-layered sub-structure, made up of concentrically fiber-reinforced layers, comprising elastin, muscle cells, and crimped collagenous fibers whose main direction is helically arranged around the vessel axis. In agreement with well-established histological in vivo measures [36] and as previously recalled (see Sect. 2.2.2), the wrapping angle $\theta_F$ of collagen fibers can be described as a function of the radial coordinate $\rho$ (Fig. 12).

The $k$th MLU ($k = 1...N$) is reduced to a homogeneous layer, comprising an anisotropic (generally with a monoclinic symmetry) non-linearly elastic material characterized by a tangent equivalent stiffness matrix $\bar{\mathbb{C}}^k(\varepsilon_F)$ (and compliance matrix $\bar{\mathbb{S}}^k = (\bar{\mathbb{C}}^k)^{-1}$). The latter is obtained by accounting for the $k$th MLU-based microstructure through a homogenization step carried out via the standard laminate theory [60, 63]. To this aim, at the radial position $\rho$, the local tangent stiffness matrix $\mathbb{C}$ is computed referring to a uni-directional collagenous tissue with the fiber chord direction $\mathbf{t}(\rho)$ inclined by $\theta_F(\rho)$ with respect to the vessel axis $z$. Accordingly, $\mathbb{C} = \mathbb{C}(\theta_F, \varepsilon_F)$, where $\theta_F = \theta_F(\rho)$ and $\varepsilon_F = \varepsilon_F(\rho)$, and thereby $\mathbb{C} = \mathbb{C}(\rho)$ at each incremental step. Since $(h_e + h_{\mathrm{IL}})/r_i \ll 1$, any curvature effect is disregarded. It is worth observing that if $\rho$ identifies a position within a EL sub-layer, $\mathbb{C}$ is described in agreement with an isotropic response, that is by involving the elastic constants $E_e$ and $v_e$ only.

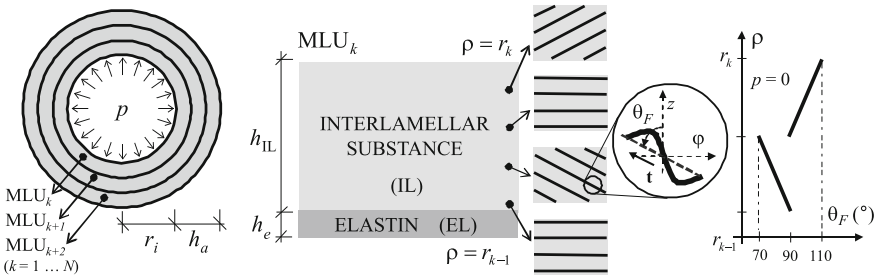


**Fig. 12** Model of the multi-layered aortic tunica media. Notation. The function $\theta_F(\rho)$ has been assumed in agreement with evidences proposed in [36]

Indicating with $\bar{S}^k_{ij}$ (respectively, $C_{ij}$ and $S_{ij}$) the components of the $6 \times 6$ compliance matrix $\bar{\mathbb{S}}^k$ (respectively of $\mathbb{C}(\rho)$ and $\mathbb{S}(\rho)$) expressed in the standard Voigt notation, the homogenized tangent compliance results from [60, 63]:

$$\begin{bmatrix} \bar{S}^k_{11} & \bar{S}^k_{12} & \bar{S}^k_{16} \\ \bar{S}^k_{21} & \bar{S}^k_{22} & \bar{S}^k_{26} \\ \bar{S}^k_{61} & \bar{S}^k_{62} & \bar{S}^k_{66} \end{bmatrix} = h_{\mathrm{IL}} \, (A^k)^{-1}, \tag{30}$$

$$\begin{bmatrix} \bar{S}^k_{31} & \bar{S}^k_{32} & \bar{S}^k_{36} \end{bmatrix} = (A^k)^{-1} \left\{ \int_{r_{k-1}}^{r_k} [\, S_{13}(\rho) \quad S_{23}(\rho) \quad S_{36}(\rho) \,] Q^k(\rho) d\rho \right\}, \tag{31}$$

$$\bar{S}^k_{33} = \frac{1}{h_{\mathrm{IL}}} \int_{r_{k-1}}^{r_k} \frac{1}{C_{33}(\rho)} \left\{ 1 - \bar{S}^k_{31} C_{13}(\rho) - \bar{S}^k_{32} C_{23}(\rho) - \bar{S}^k_{36} C_{63}(\rho) \right\} d\rho, \tag{32}$$

$$\begin{bmatrix} \bar{S}^k_{44} & \bar{S}^k_{45} \\ \bar{S}^k_{54} & \bar{S}^k_{55} \end{bmatrix} = \frac{1}{h_{\mathrm{IL}}} \int_{r_{k-1}}^{r_k} \begin{bmatrix} S_{44}(\rho) & S_{45}(\rho) \\ S_{54}(\rho) & S_{55}(\rho) \end{bmatrix} d\rho, \tag{33}$$

where

$$Q^k(\rho) = \begin{bmatrix} C_{11}(\rho) & C_{12}(\rho) & C_{16}(\rho) \\ C_{21}(\rho) & C_{22}(\rho) & C_{26}(\rho) \\ C_{61}(\rho) & C_{62}(\rho) & C_{66}(\rho) \end{bmatrix}, \qquad A^k = \int_{r_{k-1}}^{r_k} Q^k(\rho) d\rho, \tag{34}$$

and where $r_{k-1}$ and $r_k$ are the minimum and the maximum radial coordinate of the $k$th MLU, respectively.

Since non-fibrous components within interlamellar space are essentially elastin and muscle cells, and the stiffness of muscle cells can be retained as comparable to the elastin's [64], as a first approximation no distinction between elastin and muscle phases is assumed. Accordingly, the computation of $\mathbb{C}(\rho)$ via Eqs. (23)–(29) can be carried out by applying the mixture rule and by letting:

$$\frac{E_M}{E_e} = \frac{\nu_M}{\nu_e} = \left( 1 - \frac{V_o}{1 - V_f} \right). \tag{35}$$

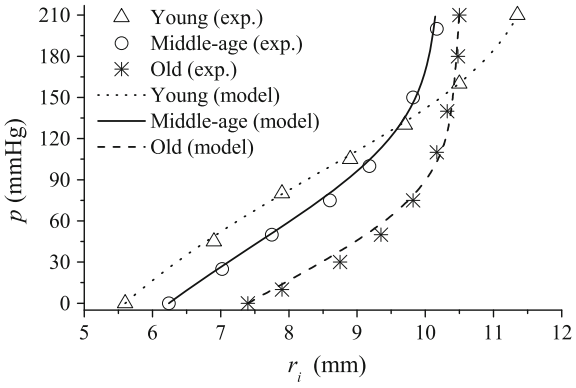


**Fig. 13** Experimental pressure $p$ vs. the internal-radius $r_i$ for human aortas at different ages [34], compared with the numerical results obtained by means of the present multiscale model. The shape of the collagen fiber centerline in the reference configuration is defined as in Eq. (20) with $\chi = 0$. Age-dependent model parameters are summarized in Table 2, whereas constant parameters are set equal to: $\ell_p = 14.5$ nm, $\ell_c = 287$ nm, $\hat{E}_o = 1$ GPa, $\hat{E} = 80$ GPa, $\eta = 22.5$, $\varepsilon_o^h = 0.1$, $\ell_{kinks} = 14$ nm, $A_m = 1.41$ nm$^2$, $T = 310.15$ K, $\mu = 1$, and $L_o = 5\,\mu$m

Due to the previous symmetry assumptions and disregarding any possible end effect, problem reduces to an axisymmetric generalized plane strain problem. In the framework of an incremental approach, the incremental elastic equilibrium solution for such a composite multi-layered thick-walled structure is obtained at each pressure variation $\dot{p}$ as briefly summarized in the Appendix, updating at each step the fiber chord direction $\mathbf{t}(\rho)$ and the fiber strain $\varepsilon_F(\rho)$ as functions of the actual macroscale strain field [8].

In Fig. 13, $p$-$r_i$ curves numerically obtained via present model are compared with the available experimental results proposed in [34]. In agreement with histological observations [31], the MTU number $N$ has been set equal to 60. Moreover, since the experimental data have been obtained on excised dead aortas, both longitudinal pre-stretch (that is, the direct strain $\varepsilon_o$, see Appendix) and smooth muscle tone have been assumed to vanish, whereas geometrical radial pre-stretch effects have been taken into account referring the fiber morphological parameters to the experimentally-analyzed undamaged aortic cross-sections at zero-load state [36].

Proposed numerical results show the effects related to the variation of some model parameters, with the aim to reproduce the evolution of the tissue mechanics induced by age. The age-dependent values of model parameters have been assumed in agreement with the evidences proposed through the recent specialized literature [3, 34, 35, 57, 65], wherein well-established data and results give indication on the evolution of some histological, geometric and mechanical characteristics in healthy human aortas. In the lack of detailed experimental data, parameters have been set within well-established physiological ranges, and their age-dependent variation has been chosen in agreement with available qualitative evidences, disregarding possible differences between the thoracic and the abdominal aortic branches.

**Table 2** Values of age-dependent model parameters for aortic media employed in numerical applications and relevant references (when available) for physiological ranges

| Age (years) | $\lambda k_{cl}$ (pN/nm) | $H_o/L_o$ (-) | $r_F/L_o$ (-) | $V_f/(1-V_o)$ (%) | $V_o$ (%) | $E_e$ (kPa) | $h_e$ (μm) | $h_a$ (mm) | $r_i\|_{p=0}$ (mm) |
|---|---|---|---|---|---|---|---|---|---|
| 20–24 | 5 | 0.425 | 0.065 | 15 | 10 | 30 | 1.4 | 0.588 | 5.6 |
| 36–42 | 10 | 0.295 | 0.032 | 20 | 30 | 80 | 1.5 | 0.630 | 6.2 |
| 71–78 | 15 | 0.225 | 0.022 | 25 | 50 | 120 | 1.65 | 0.693 | 7.4 |
| Ref. | | [36] | [36] | [66] | [66] | [35] | [35] | [35] | [34] |

Experience-based age-dependent aortic features are reported in the following, together with the corresponding evolution trends for the physically-based parameters introduced in the present model:

- Unloaded aortic radius [34, 65] and media thickness [65] increase with age. Physiological ranges are about 5.5-8.65 mm and 0.44-0.76 mm, respectively. Accordingly, $r_i|_{p=0}$ and $h_a$ increase with age.
- Elastin stiffness increases in men, due to increasing glycation with age [35], in the range 30–280 kPa. Thereby, $E_e$ increases with age.
- The stiffness of collagenous constituents at high pressure (when the collagen fibers are straightened) increases with age [35], indicating a higher stiffness of the collagen fibrils, that is $E_f$. Since the genetic pattern of healthy people is practically constant in time, it is unlikely to believe that this stiffening behavior is related to variations in the nanoscale structure of collagen molecules. Thereby, variations in $E_f$ are associated with the alteration of cross-link stiffness and/or occurrence, that is with the variation of $\lambda k_{cl}$, which increases with age. This is fully in agreement with the experimental results from [57].
- With increasing age, collagen-induced stiffening effects occur at lower pressure levels during the cardiac cycle [35]. In agreement with present microscale results (see Fig. 10), this evidence can be associated with a reduced aspect ratio $H_o/L_o$ of the collagen fibers, which then results to be inversely proportional to age.
- The stiffness of collagenous constituents at very low physiological pressure decreases with age [65]. As shown in Fig. 10, a reduction in stiffness of collagenous constituents at small strains can be associated with either more crimped or thinner fibers. In agreement with the previous evidences, the occurrence of fibers more crimped has been excluded, associating the present finding to a reduced value of the collagen fiber radius. Thereby, ratio $r_F/L_o$ decreases with age.
- Dry weight of the aortic wall decreases with age (about four or five times, [66]) despite of the increase of the aortic thickness [65]. Therefore, aortic water content (non-solid matter) increases with age, leading to the decrease of the absolute amount of elastin and collagen. On the other hand, the increase (about three times) of the relative amount of collagen with respect to the non-collagenous solid matter has been reported [66]. Accordingly, $V_o$ increases with age, as well as also $V_f/(1-V_o)$.

In agreement with previous considerations, parameters employed in proposed numerical applications are chosen as summarized in Table 2.

Figure 13 clearly shows that proposed model is able to reproduce the mean experimental $p$-$r_i$ curves associated with young (20–24 years), middle-age (36–42 years), and old (71–78 years) subjects. Although values of model parameters are chosen only in agreement with well-established trends and there is no quantitative relationships with the available experiments, the model reveals to be attractive and potentially effective in relating tissue structure at different scales and its evolution to the tissue macroscopic mechanical behavior.

## 8 Conclusions

In the present paper, a structural multiscale elastic formulation for modeling soft collagenous tissues has been presented, based on the approach proposed and applied by authors in [8, 51]. To this aim, single-scale models of collagenous bio-structures at very different length scales have been introduced, addressing molecules (nanoscale), fibrils (mesoscale) and crimped fibers (microscale). Following a multiscale structural rationale, that allows to account for the hierarchical multiscale arrangement of the constituents within tissues, these models have been integrated by means of consistent inter-scale relationships and homogenization arguments, leading to an accurate macroscale description of soft collagenous tissues.

Soundness and effectiveness of the present approach have been proved by recovering a number of well-established evidences at different length scales, without the use of phenomenological descriptions. It is shown that proposed single-scale models are able to reproduce the transition from entropic-to-energetic mechanisms at the nanoscale, the effects of inter-molecular cross-links on fibril mechanics, and the coupling between material and geometric non-linearities affecting the deformation process of crimped collagen fibers. Moreover, available experimental data on the biomechanical response of tendons and aortas have been compared with the numerical results obtained by the macroscale model, highlighting an excellent agreement. Such a capability arises from the structural multiscale approach herein adopted, that allows to account for material and geometrical non-linearities at different scales, as well as for nanoscale mechanisms. In fact, as proved in [8], a structural approach involving only microscale mechanisms is generally not able to recover accurately, for different strain levels, the non-linear mechanical response of soft collagenous tissues.

Following the proposed approach, few and experimentally measurable model parameters are introduced. Thereby, the effects of altered histological features on tissue mechanics can be straightforwardly investigated. For instance, different microscale fiber geometric features allow to explain the variability in constitutive response experienced when data measured on different specimens of rat tail tendons are compared. Moreover, the age-dependent evolution of aortic mechanical behavior has been accurately reproduced, simply by incorporating the well-documented features of age-dependent tissue remodeling.

Therefore, multiscale structural approaches allow to implement numerical simulations, that are patient-specific not only for the geometric description of tissues and organs, but also in terms of tissue constitutive properties. This opens to the possibility of numerically investigating the effects of histological and biochemical rearrangement on the mechanics of an organ, as well as of estimating, in an inverse-like scheme, the values of histo-mechano-chemical features by means of non-invasive techniques. Accordingly, among the available modeling approaches for the analysis of soft tissues, the structural multiscale rationale can be retained as the most promising for conceiving and developing groundbreaking virtual tools, allowing to improve diagnosis and to assess customized clinical treatments.

**Acknowledgments** Authors would like to thank Professor Franco Maceri for valuable suggestions and fruitful discussions on this paper.

This work was developed within the framework of Lagrange Laboratory, a European research group comprising CNRS, CNR, the Universities of Rome "Tor Vergata", Calabria, Cassino, Pavia, and Salerno, Ecole Polytechnique, University of Montpellier II, ENPC, LCPC, and ENTPE.

## Appendix

The incremental elastic equilibrium solution for the multi-layered aortic cylinder, comprising $N$ identical media lamellar units (MLUs) and loaded with a uniform internal pressure increment $\dot{p}$, is herein briefly reported. Reference is made to the linearly elastic solution proposed in [67], considering the problem as an axisymmetric generalized plane strain problem, characterized by a given non-vanishing constant direct strain increment $\dot{\varepsilon}_o$ along the cylinder axis $z$. Accordingly, for the $k$th MLU, the incremental components of the displacement field in a cylindrical system of coordinates result in

$$\dot{u}_\rho^k = A_1^k \rho^{\alpha_k} + A_2^k \rho^{-\alpha_k} + \dot{\varepsilon}_o a_1^k \rho + B^k a_2^k \rho^2, \tag{36}$$

$$\dot{u}_\varphi^k = B^k \rho z, \tag{37}$$

$$\dot{u}_z^k = \dot{\varepsilon}_o z. \tag{38}$$

The non-trivial increments of strain components are

$$\dot{\varepsilon}_\rho^k = \frac{\partial \dot{u}_\rho^k}{\partial \rho}, \qquad \dot{\varepsilon}_\varphi^k = \frac{\dot{u}_\rho^k}{\rho}, \qquad \dot{\gamma}_{z\varphi}^k = B^k \rho, \tag{39}$$

and the components of stress increments are

$$\dot{\sigma}_\rho^k = A_1^k \beta_{\rho 1}^k \rho^{\alpha_k - 1} + A_2^k \beta_{\rho 2}^k \rho^{-\alpha_k - 1} + \dot{\varepsilon}_o \beta_{\rho 3}^k + B^k \beta_{\rho 4}^k \rho, \tag{40}$$

$$\dot{\sigma}_{\varphi}^{k} = A_1^k \beta_{\varphi 1}^k \rho^{\alpha_k - 1} + A_2^k \beta_{\varphi 2}^k \rho^{-\alpha_k - 1} + \dot{\varepsilon}_o \beta_{\varphi 3}^k + B^k \beta_{\varphi 4}^k \rho, \tag{41}$$

$$\dot{\sigma}_{z}^{k} = A_1^k \beta_{z 1}^k \rho^{\alpha_k - 1} + A_2^k \beta_{z 2}^k \rho^{-\alpha_k - 1} + \dot{\varepsilon}_o \beta_{z 3}^k + B^k \beta_{z 4}^k \rho, \tag{42}$$

$$\dot{\tau}_{z\varphi}^{k} = A_1^k \beta_{\gamma 1}^k \rho^{\alpha_k - 1} + A_2^k \beta_{\gamma 2}^k \rho^{-\alpha_k - 1} + \dot{\varepsilon}_o \beta_{\gamma 3}^k + B^k \beta_{\gamma 4}^k \rho, \tag{43}$$

where

$$\beta_{q1}^k = \bar{C}_{g2}^k + \alpha_k \bar{C}_{g3}^k, \qquad \beta_{q2}^k = \bar{C}_{g2}^k - \alpha_k \bar{C}_{g3}^k, \tag{44}$$

$$\beta_{q3}^k = \bar{C}_{g1}^k + (\bar{C}_{g2}^k + \bar{C}_{g3}^k) a_1^k, \qquad \beta_{q4}^k = \bar{C}_{g6}^k + (\bar{C}_{g2}^k + 2\bar{C}_{g3}^k) a_2^k, \tag{45}$$

with the index $q = z, \varphi, \rho, \gamma$ corresponding to the $g$-index values $g = 1, 2, 3, 6$, respectively, and with

$$\alpha_k^2 = \bar{C}_{22}^k / \bar{C}_{33}^k, \tag{46}$$

$$a_1^k = (\bar{C}_{12}^k - \bar{C}_{13}^k)/[\bar{C}_{33}^k (1 - \alpha_k^2)], \qquad a_2^k = (\bar{C}_{26}^k - 2\bar{C}_{36}^k)/[\bar{C}_{33}^k (4 - \alpha_k^2)], \tag{47}$$

$\bar{C}_{ij}^k$ denoting the $(i,j)$ component of the stiffness matrix $\mathbb{C}^k$ for the $k$th MLU.

It is worth pointing out that during the deformation path both strain and stress components, and thereby also the strain-dependent MTU material properties, are $z$- and $\varphi$-independent.

Assuming the MLUs as perfectly bonded layers, the $3N$ unknown constants $A_1^k$, $A_2^k$, $B^k$ (with $k = 1...N$) are solved by imposing the following $3(N-1)$ continuity conditions at the MLU's interfaces:

$$\dot{u}_{\rho}^{k}(r_k) = \dot{u}_{\rho}^{k+1}(r_k), \qquad \dot{u}_{\varphi}^{k}(r_k) = \dot{u}_{\varphi}^{k+1}(r_k), \qquad \dot{\sigma}_{r}^{k}(r_k) = \dot{\sigma}_{r}^{k+1}(r_k), \tag{48}$$

and the three equilibrium incremental relationships:

$$\dot{\sigma}_r(r_i) = -\dot{p}, \qquad \dot{\sigma}_r(r_i + h_a) = 0, \qquad 2\pi \sum_{k=1}^{N} \int_{r_{k-1}}^{r_k} \rho^2 \dot{\tau}_{z\varphi}^{k} d\rho = 0, \tag{49}$$

the latter prescribing the average torque related to the tangential stress increment $\dot{\tau}_{z\varphi}$ to be zero.

## References


1. van Holde, K.E., Matthews, C.: Biochemistry. Benjamin/Cummings Publishing Company Inc., Menlo Park (1995)
2. Fratzl, P.: Collagen: Structure and Mechanics. Springer, New York (2008)
3. Bruel, A., Oxlund, H.: Changes in biomechanical properties, composition of collagen and elastin, and advanced glycation endproducts of the rat aorta in relation to age. Atherosclerosis **127**, 155–165 (1996)

4. Bruel, A., Ørtoft, G., Oxlund, H.: Inhibition of cross-links in collagen is associated with reduced stiffness of the aorta in young rats. Atherosclerosis **140**, 135–145 (1998)
5. Mao, J.R., Bristow, J.: The Ehlers–Danlos syndrome: on beyond collagens. J. Clin. Invest. **107**, 1063–1069 (2001)
6. Carmo, M., Colombo, L., Bruno, A., Corsi, F.R.M., Roncoroni, L., Cuttin, M.S., Radice, F., Mussini, E., Settembrini, P.G.: Alteration of elastin, collagen and their cross-links in abdominal aortic aneurysms. Eur. J. Vasc. Endovasc. Surg. **23**, 543–549 (2002)
7. Järvinen, T.A.H., Järvinen, T.L.N., Kannus, P., Józsa, L., Järvinen, M.: Collagen fibres of the spontaneously ruptured human tendons display decreased thickness and crimp angle. J. Orthop. Res. **22**, 1303–1309 (2004)
8. Maceri, F., Marino, M., Vairo, G.: A unified multiscale mechanical model for soft collagenous tissues with regular fiber arrangement. J. Biomech. **43**, 355–363 (2010)
9. Buehler, M.J., Wong, S.Y.: Entropic elasticity controls nanomechanics of single tropocollagen molecules. Biophys. J. **93**, 37–43 (2007)
10. Marko, J.F., Siggia, E.D.: Stretching DNA. Macromolecules **28**, 8759–8770 (1995)
11. MacKintosh, F.C., Käs, J., Janmey, P.A.: Elasticity of semiflexible biopolymer networks. Phys. Rev. Lett. **75**, 4425–4428 (1995)
12. Sun, Y.L., Luo, Z.P., Fertala, A., An, K.N.: Direct quantification of the flexibility of type I collagen monomer. Biochem. Biophys. Res. Commun. **295**, 382–386 (2002)
13. Wang, M.D., Yin, H., Landick, R., Gelles, J., Block, S.M.: Stretching DNA with optical tweezers. Biophys. J. **72**, 1335–1346 (1997)
14. Holzapfel, G.A., Ogden, R.W.: On the bending and stretching elasticity of biopolymer filaments. J. Elast. **104**, 319–342 (2010)
15. Maceri, F., Marino, M., Vairo, G.: Elasto-damage modeling of biopolymer molecules response. Comput. Model. Eng. Sci. (2012, to appear) ISSN:1526-1492
16. Gautieri, A., Buehler, M.J., Redaelli, A.: Deformation rate controls elasticity and unfolding pathway of single tropocollagen molecules. J. Mech. Behav. Biomed. Mat. **2**, 130–137 (2009)
17. Eyre, D.R., Weis, M.A., Wu, J.J.: Advances in collagen cross-link analysis. Methods **45**(1), 65–74 (2008)
18. Orgel, J.P.R.O., Irving, T.C., Miller, A., Wess, T.J.: Microfibrillar structure of type I collagen in situ. Proc. Nat. Acad. Sci. USA **103**, 9001–9005 (2006)
19. Petruska, J.A., Hodge, A.J.: A subunit model for the tropocollagen macromolecule. Proc. Natl Acad. Sci. USA **51**, 871–876 (1964)
20. Pins, G.D., Christiansen, D.L., Patel, R., Silver, F.H.: Self-assembly of collagen fibers. Influence of fibrillar alignment and decorin on mechanical properties. Biophys. J. **73**, 2164–2172 (1997)
21. Redaelli, A., Vesentini, S., Soncini, M., Vena, P., Mantero, S., Montevecchi, F.M.: Possible role of decorin glycosaminoglycans in fibril to fibril force transfer in relative mature tendons—a computational study from molecular to microstructural level. J. Biomech. **36**, 1555–1569 (2003)
22. Craig, A.S., Birtles, M.J., Conway, J.F., Parry, D.A.: An estimate of the mean length of collagen fibrils in rat tail-tendon as a function of age. Connect. Tissue Res. **19**, 51–62 (1989)
23. Provenzano, P.P., Vanderby, R.J.: Collagen fibril morphology and organization: implications for force transmission in ligament and tendon. Matrix Biol. **25**, 71–84 (2006)
24. Fessel, G., Snedeker, J.G.: Equivalent stiffness after glycosaminoglycan depletion in tendon—an ultra-structural finite element model and corresponding experiments. J. Theor. Biol. **268**, 77–83 (2011)
25. Martini, F.H., Timmons, M.J., Tallitsch, R.B.: Human Anatomy. Prentice Hall, Englewood Cliffs (1994)
26. Sasaki, N., Odajima, S.: Elongation mechanism of collagen fibrils and force–strain relations of tendon at each level of structural hierarchy. J. Biomech. **29**, 1131–1136 (1996)
27. Hansen, K.A., Weiss, J.A., Barton, J.K.: Recruitment of tendon crimp with applied tensile strain. J. Biomech. Eng. **124**, 72–77 (2002)

28. Yamamoto, E., Kogawa, D., Tokura, S., Hayashi, K.: Biomechanical response of collagen fascicles to restressing after stress deprivation during culture. J. Biomech. **40**, 2063–2070 (2007)
29. Kannus, P.: Structure of the tendon connective tissue. Scand. J. Med. Sci. Sports **10**, 312–320 (2000)
30. Silver, F.H., Freeman, J.W., Horvath, I., Landis, W.J.: Molecular basis for elastic energy storage in mineralized tendon. Biomacromolecules **2**, 750–756 (2001)
31. Wolinsky, H., Seymour, G.: A lamellar unit of aortic medial structure and function in mammals. Circ. Res. **20**, 99–111 (1967)
32. Clark, J.M., Glagov, S.: Transmural organization of the arterial media—the lamellar unit revisited. Arteriosclerosis **5**, 19–34 (1985)
33. Wolinsky, H., Seymour, G.: Comparison of abdominal and thoracic aortic medial structure in mammals. Circ. Res. **25**, 677–686 (1969)
34. Hallock, P., Benson, I.C.: Studies on the elastic properties of human isolated aorta. J. Clin. Invest. **16**, 595–602 (1937)
35. Åstrand, H., Stålhand, J., Karlsson, M., Sonesson, B., Länne, T.: In vivo estimation of the contribution of elastin and collagen to the mechanical properties in the human abdominal aorta: effects of age and sex. J. Appl. Phys. 110:176–187 (2011)
36. O'Connell, M.K., Murthy, S., Phan, S., Xu, C., Buchanan, J., Spilker, R., Dalman, R.L., Zarins , C.K., Denk, W., Taylor, C.A.: The three-dimensional micro- and nanostructure of the aortic medial lamellar unit measured using 3D confocal and electron microscopy imaging. Matrix Biol. **27**, 171–181 (2008)
37. Behmoaras, J., Osborne-Pellegrin, M., Gauguier, D., Jacob, M.P.: Characteristics of the aortic elastic network and related phenotypes in seven inbred rat strains. Am. J. Physiol. Heart. Circ. Physiol. **288**, 769–777 (2005)
38. Merrilees, M., Tiang, K.M., Scott, L.: Changes in collagen fibril diameters across artery walls including a correlation with glycosaminoglycan content. Connect. Tissue Res. **16**, 237–257 (1987)
39. Rachev, A., Stergiopulos, N., Meister, J.J.: Theoretical study of dynamics of arterial wall remodeling in response to changes in blood pressure. J. Biomech. **29**, 635–642 (1996)
40. Zhang, W., Herrera, C., Atluri, S.N., Kassab, G.S.: The effect of longitudinal pre-stretch and radial constraint on the stress distribution in the vessel wall: a new hypothesis. Mech. Chem. Biosyst. **2**, 41–52 (2005)
41. Kassab, G.S.: Biomechanics of the cardiovascular system: the aorta as an illustratory example. J. R. Soc. Interface **3**, 719–740 (2006)
42. Fung, Y.C.: Biorheology of soft tissues. Biorheology **10**, 199–212 (1973)
43. Yin, L., Elliott, D.M.: A biphasic and transversely isotropic mechanical model for tendon: application to mouse tail fascicles in uniaxial tendons. J. Biomech. **37**, 907–916 (2004)
44. Comninou, M., Yannas, I.V.: Dependance of stress–strain nonlinearity of connective tissues on the geometry of collagen fibers. J. Biomech. **9**, 427–433 (1976)
45. Lanir, Y.: A structural theory for the homogeneous biaxial stress–strain relationships in flat collagenous tissues. J. Biomech. **12**, 423–436 (1979)
46. Freed, A.D., Doehring, T.C.: Elastic model for crimped collagen fibrils. J. Biomech. Eng. **127**, 587–593 (2005)
47. Holzapfel, G.A., Gasser, T.C., Ogden, R.W.: A new constitutive framework for arterial wall mechanics and a comparative study of material models. J. Elast. **61**, 1–48 (2000)
48. Holzapfel, G.A., Gasser, T.C., Stadler, M.: A structural model for the viscoelastic behavior of arterial walls: continuum formulation and finite element analysis. Eur. J. Mech. A Solids **21**, 441–463 (2002)
49. Ciarletta, P., Micera, S., Accoto, D., Dario, P.: A novel microstructural approach in tendon viscoelastic modelling at the fibrillar level. J. Biomech. **39**, 2034–2042 (2006)
50. Tang, H., Buehler, M.J., Moran, B.: A constitutive model of soft tissue: from nanoscale collagen to tissue continuum. Ann. Biomed. Eng. **37**, 1117–1130 (2009)

51. Maceri, F., Marino, M., Vairo, G.: From cross-linked collagen molecules to arterial tissue: a nano-micro-macroscale elastic model. Acta Mech. Solida Sin. **23**(S1), 98–108 (2010)
52. Marino, M., Vairo, G.: Stress and strain localization in stretched collagenous tissues via a multiscale modeling approach. Comput. Methods Biomech. Biomed. Engin. (2012). doi:10.1080/10255842.2012.658043
53. Maceri, F., Marino, M., Vairo, G.: An insight on multiscale tendon modeling in muscle-tendon integrated behavior. Biomech. Model. Mechanobiol. **11**, 505–517 (2011)
54. Bozec, L., Horton, M.: Topography and mechanical properties of single molecules of type I collagen using atomic force microscopy. Biophys. J. **88**, 4223–4231 (2005)
55. Holmes, D.F., Graham, H.K., Trotter, J.A., Kadler, K.E.: STEM/TEM studies of collagen fibril assembly. Micron **32**, 273–285 (2001)
56. Buehler, M.J.: Nanomechanics of collagen fibrils under varying cross-link densities: atomistic and continuum studies. J Mech. Behav. Biomed. Mat. **1**, 59–67 (2008)
57. Bailey, A.J.: Molecular mechanisms of ageing in connective tissues. Mech. Ageing Dev. **122**, 735–755 (2001)
58. Couppé, C., Hansen, P., Kongsgaard, M., Kovanen, V., Suetta, C., Aagaard, P., Kjær, M., Magnusson, S.P.: Mechanical properties and collagen cross-linking of the patellar tendon in old and young men. J. Appl. Physiol. 107:880–886 (2009)
59. Marino, M., Vairo, G.: Equivalent stiffness and compliance of curvilinear elastic fibers. In: Maceri, F., Frémond, M. (eds.) Mechanics, Models and Methods in Civil Engineering. Lecture Notes in Applied & Computational Mechanics, vol. 61, pp. 309–332. Springer, Berlin (2011)
60. Kollar, L.P., Springer, G.S.: Mechanics of Composite Structures. Cambridge University Press, Cambridge (2003)
61. Screen, H.R.C., Lee, D.A., Bader, D.L., Shelton, J.C.: An investigation into the effects of the hierarchical structure of tendon fascicles on micromechanical properties. Proc. Inst. Mech. Eng. **218**, 109–119 (2004)
62. Lavagnino, M., Arnoczky, S.P., Caballero, O., Kepich, E., Haut R., C.: A finite element model predicts the mechanotrasduction of tendon cells to cyclic tensile loading. Biomech. Model. Mechanobiol. **7**, 405–416 (2008)
63. Auricchio, F., Sacco, E., Vairo, G.: A mixed FSDT finite element for monoclinic laminated plates. Comput. Struct. **84**, 624–639 (2006)
64. Zulliger, M.A., Rachev, A., Stergiopulos, N.: A constitutive formulation of arterial mechanics including vascular smooth muscle tone. Am. J. Physiol. Heart Circ. Physiol. **287**, 1335–1343 (2004)
65. Åstrand, H., Rydén-Ahlgren, Å ., Sandgren, T., Länne, T.: Age-related increase in wall stress of the human abdominal aorta: an in vivo study. J. Vasc. Surg. 42:926–931 (2005)
66. Cattell, M.A., Anderson, J.C., Hasleton, P.S.: Age-related changes in amounts and concentrations of collagen and elastin in normotensive human thoracic aorta. Clin. Chim. Acta **245**, 73–84 (1996)
67. Marklund, E., Varna, J.: Modeling the effect of helical fiber structure on wood fiber composite elastic properties. Appl. Compos. Mater. **16**, 245–262 (2009)